Power Electronic Systems
Laboratory

IEEE Transactions on Industrial Electronics, Vol. 61, No. 1, pp. 231-242, January 2014

3-D Electromagnetic Modeling of EMI Input Filters

I. Kovacevic,
T. Friedli,
A. Müsing,
J. W. Kolar

Eidgenössische Technische Hochschule Zürich
Swiss Federal Institute of Technology Zurich

3-D Electromagnetic Modeling of EMI Input Filters

Ivana F. Kovačević, *Student Member, IEEE*, Thomas Friedli, *Member, IEEE*,
Andreas M. Muesing, *Member, IEEE*, and Johann W. Kolar, *Fellow, IEEE*

***Abstract*—In this paper, a novel 3-D electromagnetic modeling approach which enables electromagnetic compatibility (EMC) analysis of power converter systems in an accurate and computationally efficient way is presented. The 3-D electromagnetic modeling approach, implemented in the EMC simulation tool GeckoEMC, is based on two numerical techniques, the partial element equivalent circuit method and the boundary integral method (PEEC–BIM). The developed PEEC–BIM coupled method enables comprehensive EMC analysis taking into account different effects of the PCB layout, self-parasitics, mutual coupling, shielding, etc., which in turn provides a detailed insight into the electromagnetic behavior of power electronic systems in advance to the implementation of hardware prototypes. The modeling features of the GeckoEMC simulation tool for virtual design of electromagnetic interference (EMI) filters and power converters is demonstrated on the examples of a single-phase two-stage EMI filter and a practical EMI filter for a single-phase PFC input stage. Good agreement between the PEEC–BIM simulation and the small signal transfer function measurement results is achieved over a wide frequency range, from dc up to 30 MHz. The EMC simulation environment enables a step-by-step EMC analysis distinguishing the impact of various electromagnetic effects on the EMI filter performance and allowing an optimal EMI filter design.**

***Index Terms*—Electromagnetic interference (EMI) filter, partial element equivalent circuit (PEEC) method, power factor correction (PFC), 3-D electromagnetic modeling, virtual prototyping.**

I. Introduction

SWITCHED-MODE power supplies (SMPSs) have been widely used for various fields of application in industrial, commercial, residential, aerospace, and military environments, following the modern trends in industry for maximum power density performance at minimum cost and ever-increasing power conversion efficiency. As the basic principle of SMPSs is fast switching of high current and voltage signals within power converter systems, different challenges and constraints arise with the design of SMPSs [1]. The compromise between efficiency and power density has to be always made and the electromagnetic interference (EMI) problems become more critical. Namely, SMPSs represent a significant EMI source due to their intrinsic switching properties and the generated EMI noise levels must be properly controlled. Moreover, electromagnetic compatibility (EMC) regulations, e.g., CIPSR 11 [2] and line-current harmonic standards, e.g., IEC 61000-3-2 (for $I_{\mathrm{n}} < 16$ A) [3], have to be satisfied. Different EMI mitigation and harmonic line current reduction techniques have been developed over the years to improve the design of SMPS to meet these standards. Generally, EMC analysis represents an important step of the overall SMPS design procedure to assure both low EMI emission and high power quality.

High power quality, i.e., a low line current distortion, is obtained by active power factor correction (PFC) circuits used as front-end in SMPS [4]. PFC circuits increase EMI noise generation in the high frequency range and in addition, the PFC input stage is the main EMI noise source for SMPS. Therefore, good EMC design is based on the understanding of EMI noise generation mechanisms and EMI noise propagation paths within power converter systems. EMC analysis of different converter topologies used in SMPS has been the topic of a lot of research. The reduction of EMI noise levels is achieved at the source-side, i.e., the SMPS, by means of improved switching schemes [5], soft-switching techniques [6], employment of fast switching devices (e.g., SiC diodes with low reverse recovery current [7], [8]), optimal layouts, etc., and additionally by EMI filtering inserted between SMPS and power lines [9]. Due to low cost and no need for control, passive EMI filters have been commonly used to increase EMI noise attenuation. However, passive components introduce additional volume and cost to the overall power converter system design and have to be properly built and placed. Furthermore, the interaction between EMI filtering components and power converter stages can degrade the main electrical functionality and introduce instabilities [10], [11].

The design of an EMI filter is not an easy task, and it has been often regarded as trial-and-error process that requires great practical experience and wide knowledge in different fields such as EMC, EMI, power converters design, and control. All EMC effects have to be taken into account simultaneously, and this makes the actual SMPS design process even more complicated. Accordingly, EMI/EMC modeling and simulation is increasing in importance and represents a valuable design approach. The main motivation of this paper is to introduce a novel 3-D CAD tool as the state-of-the-art for EMI filter design and EMC analysis of power converter systems [12].

In Section II, the EMI filter design requirements are discussed using the example of a single-phase PFC input stage. In Section III, an EMC simulation platform for the virtual design of EMI input filters, GeckoEMC, is introduced. It is based on 3-D electromagnetic modeling using two numerical techniques, the Partial Element Equivalent Circuit (PEEC) method and the PEEC-Boundary Integral Method (PEEC–BIM). The

Manuscript received October 24, 2012; accepted December 12, 2012. Date of publication January 24, 2013; date of current version July 18, 2013.

I. F. Kovačević, A. M. Muesing, and J. W. Kolar are with the Power Electronic Systems Laboratory, ETH Zurich, 8092 Zurich, Switzerland (e-mail: kovacevic@lem.ee.ethz.ch; muesing@lem.ee.ethz.ch; kolar@lem.ee.ethz.ch).

T. Friedli is with ABB Switzerland, Ltd., CH-8050 Zurich, Switzerland (e-mail: thomas.friedli@ieee.org).

Color versions of one or more of the figures in this paper are available online at http://ieeexplore.ieee.org.

Digital Object Identifier 10.1109/TIE.2013.2242422

developed PEEC-based modeling method is verified by transfer function measurements of single-phase two-stage EMI filter circuits. A detailed 3-D PEEC–BIM modeling of a practical EMI filter for a PFC input stage, i.e., with a PCB layout defined by the space constraints, is presented in Section IV. The capabilities of the proposed PEEC–BIM method are demonstrated in a step-by-step way, distinguishing the influence of different passive components on EMI filter performance. Section V summarizes the advantages of the developed 3-D EMC modeling environment.

II. EMI/EMC Modeling

The switching properties of SMPS introduce both conducted and radiated electromagnetic noise signals that may interfere with power supply lines and other surrounding devices, leading to general system malfunction. While radiated EMI noise can be significantly reduced by proper shielding, an EMI filter has to be implemented between power lines and SMPS to reduce the conducted noise levels to meet the EMC standard limits. Accordingly, the prediction of high frequency behavior of power converter systems is necessary to mitigate these EMI noise disturbances in the frequency range of interest, e.g., the frequency range specified by European CIPSR standards for the conducted EMI emission extends from 150 kHz to 30 MHz, and to find an optimal EMI filter configuration [13], [14].

EMI analysis is commonly performed in the following steps:

- defining EMI noise sources, i.e., identifying fast rates of change of currents and voltages, $\mathrm{d}i/\mathrm{d}t$ and/or $\mathrm{d}v/\mathrm{d}t$, respectively,
- identifying the noise propagation paths, i.e., common and differential mode conduction paths,
- implementing different EMI mitigation techniques including the design of an EMI filter, and finally
- identification of all parasitic effects that occur at higher frequencies, i.e., above a few MHz, and lead to unwanted electromagnetic behavior.

This last step can be seen as the most difficult, as the prediction of self- and mutual–parasitic effects is not a straightforward task and a general tool for calculation and modeling of these effects still does not exist. Specifically, it has been shown that the design of an EMI filter involves not just the selection of EMI filter components so that the required attenuation is satisfied, but that also the PCB layout and component placement is important for achieving the desired performance.

A. State-of-the-Art

Stringent EMC regulations have motivated power electronics engineers to dedicate a lot of research to the topic of EMI HF performance of power converters and the design of EMI filters. Comprehensive research about EMI analysis, investigating the influence of heatsink, PCB layout, and mutual coupling effects, was carried out in [12], [15]–[20]. In the published work, the influence of the self-/mutual–parasitics is extracted from the high frequency circuit models of passive components and then calculated by means of the network circuit approach, i.e., modeling an EMI input filter as a two-port network and then, measuring or simulating (in Maxwell Q3D as in [11], [21]) the S, Z, or Y network parameters. This approach can be seen as complex since a proper equivalent circuit that corresponds to the real physical behavior has to be determined and it requires a set of measurements to be performed to correctly characterize all mutual couplings within a power converter system. The second approach to EMI/EMC modeling is via numerical methods [22], [23].

The most well-known numerical techniques for power electronics applications are the finite element (FE) method (e.g., [24]) and the partial element equivalent circuit (PEEC) method (e.g., [25]). The main advantage of the PEEC method in comparison to the FE method is the modeling of a set of conductors in air with longitudinal size much longer than the other two dimensions, as it is the case with PCB layouts [26], e.g., a PCB track with 0.35 μm thickness and several centimeters length. It was shown that the PEEC method is a fast and accurate tool for EMC analysis of power converter systems, which can be regarded as a circuit-field coupled problem.

However, the lack of accurate PEEC-based modeling of nonlinear properties of magnetic cores used in inductors and transformers has been the main obstacle to developing a 3-D CAD tool for the prediction of EMI/EMC performances of power electronic components and full power converter circuits [12], [20]. For this reason, an extended PEEC-based modeling technique, the coupled PEEC–boundary integral method (PEEC–BIM), has been developed [27], [28] and implemented in an EMC simulation tool, GeckoEMC [29]. The modeling features of GeckoEMC were presented [30]–[32] and verified by impedance and transfer function measurements. In comparison to other commercial EMC simulation software, GeckoEMC enables 3-D virtual prototyping of complete power converter systems simultaneously taking different effects into account: the electromagnetic influence of magnetic cores, self-parasitics, mutual-coupling between components, etc. In this paper, the PEEC–BIM modeling of different practical EMI input filter circuits is investigated proving the usefulness of the EMC simulation tool for detailed EMC analysis of EMI filters, and also its applicability to EMC modeling of power converter systems.

B. EMI Noise Mechanism

EMI noise sources within power converters are the pulsating currents of the critical PCB trace loops $(\mathrm{d}i/\mathrm{d}t)$ and the pulsating voltages of the phase nodes $(\mathrm{d}v/\mathrm{d}t)$. The common (CM) and differential (DM) noise sources and the corresponding noise propagation paths are illustrated in Fig. 1 for a single-phase PFC boost rectifier. The current and voltage waveforms can be represented by their EMI spectrum which specifies the amount of filtering that is required to meet EMC regulations. The Line Impedance Stabilization Network (LISN) connected at the output of SMPS is used to measure and characterize its EMI behavior providing a defined (standardized) 50 Ω HF impedance from the ac power source [33].

The EMC analysis of the PFC boost circuits has been extensively studied in literature [18], [19], [21], [34]–[36]. The EMI noise generation and propagation is illustrated in Fig. 1

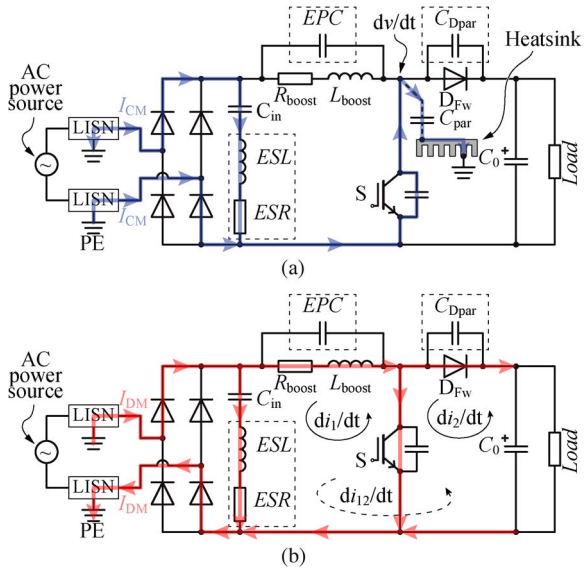

Fig. 1. PFC boost rectifier connected to LISNs (doted blocks: self-parasitic components): (a) CM noise propagation paths, and (b) DM noise propagation paths.

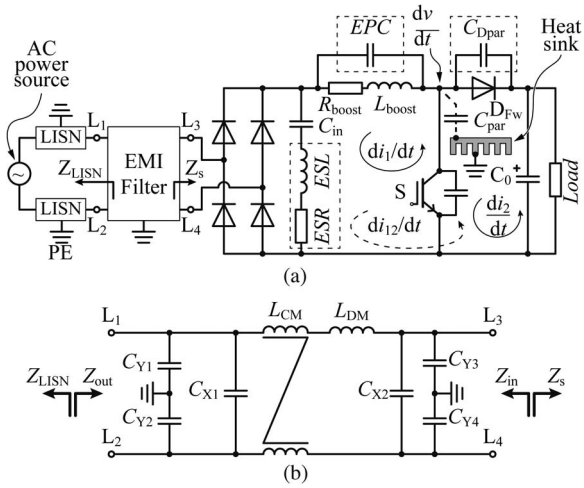

Fig. 2. (a) PFC boost rectifier with EMI input filter, and (b) EMI input filter topology.

for a PFC boost rectifier operating in continuous conduction mode (CCM). The CM noise is associated with the fast voltage change of the switch nodes, i.e., the drain of the MOSFET $\mathrm{d}v_\mathrm{D}/\mathrm{d}t$, and propagates between the power lines (L and N) and the common ground path (PE) via the parasitic capacitive coupling C_par, cf. Fig. 1(a). The total CM parasitic capacitance includes also the parasitic capacitance of the load, which is not shown in Fig. 1(a).

The DM noise is caused by the normal switching operation of the converter and propagates between the phase (L) and neutral (N) line, cf. Fig. 1(b). It was shown that the DM and CM noise can be measured separately by means of CM/DM noise separators so that the design procedures of CM and DM EMI input filters can be decoupled [33], [37]. In the case of the unbalanced propagation paths between the converter and the LISNs, mix-mode (MM) noise can occur, which is not shown in Fig. 1 for the sake of brevity [38].

C. EMI Filter Design

The design of the CM and DM EMI input filter has to be performed with respect to the input impedance mismatch rule described in [33], [39], i.e., the mismatch between the impedance of noise source Z_s and the input filter impedance Z_in, and between the LISN impedance, i.e., $Z_\mathrm{LISN,CM} = 25\ \Omega$, $Z_\mathrm{LISN,DM} = 100\ \Omega$ and the filter output impedance Z_out [18], [21]. Furthermore, the coupling between the EMI filter and the PFC boost input stage can have significant influence on EMI spectrum distribution [20]. EMC analysis of CCM PFC boost converter was shown that the DM noise source impedance is equal to the impedance of the boost inductor Z_boost, and that the CM noise source impedance is C_par, the capacitance between the case of the power semiconductor switch and the heatsink, that is typically connected to the earth of the ac power supply for safety reasons.

The commonly used input filter topology is presented in Fig. 2. It consists of two balanced CM capacitor stages, $C_{\mathrm{Y}_{1-4}}$, DM capacitors $C_{\mathrm{X}_{1-2}}$, CM inductor L_CM, and DM inductor L_DM. The leakage inductance of the CM choke, $L_\mathrm{CM,DM}$, can be used for the suppression of DM noise and hence it should be included in the design of the total DM inductance. The value of Y-capacitors $C_{\mathrm{Y}_{1-4}}$ have to be specified according to the maximum ground current given by the safety regulations. Besides the fact that the boost inductor L_boost determines the DM noise spectrum, it can also be included in the first stage of a DM EMI input filter [40]. Likewise, the input capacitor C_in in Fig. 2 is used as a part of the DM filter to bypass high frequency DM noise current. However, the high values of C_in negatively affect the power factor correction so special care must be taken with the design and placement of the filter capacitor after the diode bridge [41].

The self-parasitics due to nonideal behavior and mutual–parasitic effects originating from the near field electromagnetic coupling between passive filter components determine the effectiveness of EMI filter in the HF range. Different parasitic cancellation techniques have been proposed to improve the frequency response of EMI filter components and also the overall HF behavior of the EMI filter as a whole. The implementation of these parasitic cancellation techniques have to be carefully performed [42]. The 3-D EMC modeling of all parasitic effects allows the evaluation of EMI filters with the same topology but different PCB layouts without the need to build different hardware prototypes and enables an optimal EMI filter realization.

III. Virtual Design of EMI Input Filters

In this section, 3-D EMC modeling based on the PEEC–BIM method is described. A brief summary of PEEC–BIM-based modeling of EMI filter components is given and an experimental example, a single-phase two-stage EMI filter circuit, is described. Then, in the following section, modeling of a practical EMI input filter for a PFC rectifier is presented.

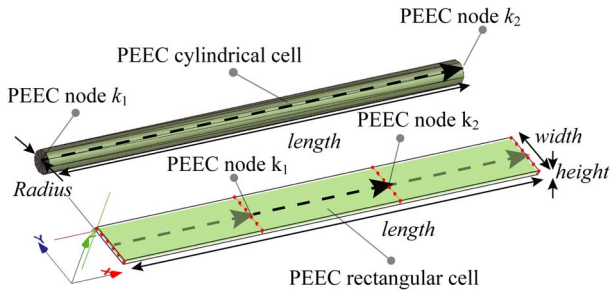

Fig. 3. PEEC–BIM model of conductors: PEEC cylindrical cell modeling a wire and PEEC rectangular cell modeling a PCB track.

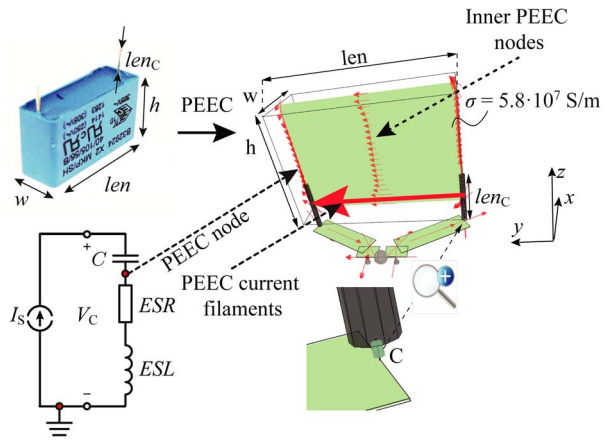

Fig. 4. PEEC–BIM model of EMI filter foil capacitors.

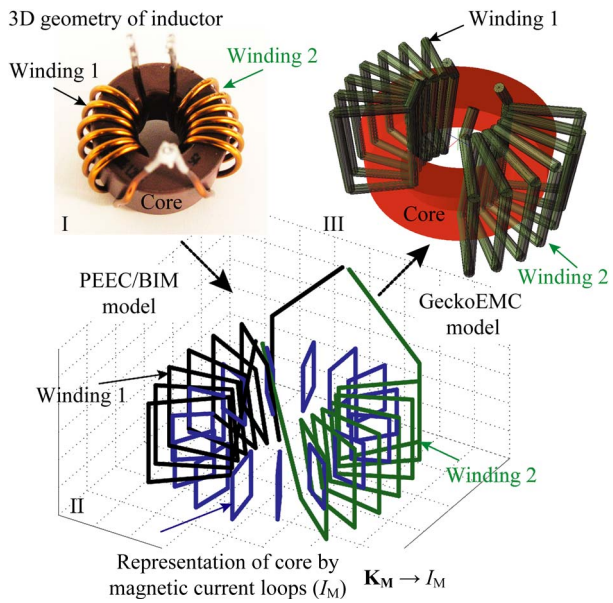

Fig. 5. PEEC–BIM model of EMI filter inductors, shown for a single-phase CM inductor.

A. Modeling of EMI Filter Components

Conductors are modeled by PEEC cells with rectangular and cylindrical geometry corresponding to 3-D PEEC models of a PCB track and a solid wire, respectively. The conductivity of the PEEC cells is equal to the conductivity of actual PCB tracks and wires. The PEEC–BIM models for passive components of EMI filter are shown in Figs. 3–5.

The passive EMI filter components can be represented by 3-D PEEC–BIM models with the same geometry as the actual components and the electric and/or magnetic properties set to fit the real HF behavior. Specifically, the 3-D PEEC model of EMI filter capacitors is a rectangular PEEC cell with the same dimensions, i.e., length × width × height, as the real capacitor while the conductivity σ and the connectors length len_C are determined to fit the equivalent series resistance ESR and equivalent series inductance ESL. The capacitance is modeled by a circuit element C added in the series to the current path between the capacitors connectors keeping a small distance between the capacitor's nodes, cf. Fig. 4. This PEEC-based representation of EMI filter capacitors also correctly models the mutual coupling effects due to the current path between the capacitor's connectors, that was verified in [31].

As mentioned previously, the PEEC-based modeling of EMI filter inductors has been seen as a more difficult task. So far, in literature, several assumptions were introduced to circumvent the problem of PEEC-based modeling of EMI filter inductors. In [22], the authors used an effective permeability factor to extract the PEEC differential mode partial inductance $L_{\mathrm{CM,DM}}$ of a common mode (CM) filter inductor. In [23], the authors ignore the presence of the magnetic core to simplify the PEEC-based model of CM inductors to perform fast EMC optimization of a power converter.

The design of practical EMI filter inductors is based on the selection of an appropriate core and winding configuration so that the inductor can withstand the rated current without saturating while simultaneously providing the required CM/DM noise attenuation. The selection of the core is typically performed according to the permeability curves $\mu_{\mathrm{r}}(f)$ given in datasheets or extracted from impedance measurements. Hence, a magnetic core can be observed as a linear homogeneous material characterized by $\mu_{\mathrm{r}}(f)$ curves (as long as the core is not operated in a highly nonlinear range). This allows the application of the linear PEEC modeling approach. Accordingly, the PEEC-Boundary Integral Method (PEEC–BIM) model of EMI filter inductors has been developed replacing the core by a surface distribution of fictitious magnetic currents $(\vec{K}_{\mathrm{M}})$, which produces the same electromagnetic field in space as the core [28]. The model was verified for toroidal cores commonly used for EMI filter inductors. Furthermore, it was proved that the electromagnetic influence of the core can be simplified by magnetic currents forming loops around the core circumference (I_{M}). The strength of these magnetic currents is higher at the core regions covered with the winding and hence, I_{M} current distribution determines the direction of stray magnetic field lines of inductors. The PEEC–BIM model of other core geometries will be implemented in the course of future research.

The 3-D PEEC–BIM models of the circuit protection components are also included in the 3-D modeling environment. Namely, as the frequency response of fuses can be represented by an R-L circuit in the frequency range up to 30 MHz, F_1 and F_2 components are represented by cylindrical PEEC cells, cf. Fig. 6, and the conductivity and length of fuse connectors are set to fit the measured HF impedance. Similarly, the thermistor NTC and the varistor RV are modeled by PEEC cells setting

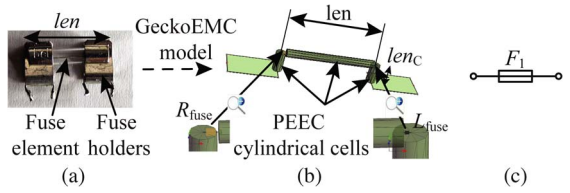

Fig. 6. Fuse circuit component: (a) a photograph, (b) PEEC model in GeckoEMC, and (c) circuit symbol.

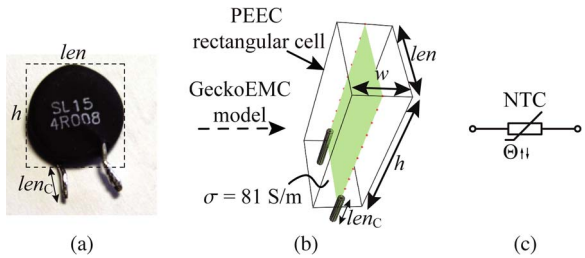

Fig. 7. Negative temperature coefficient (NTC) thermistor component: (a) a photograph, (b) PEEC model in GeckoEMC, and (c) circuit symbol.

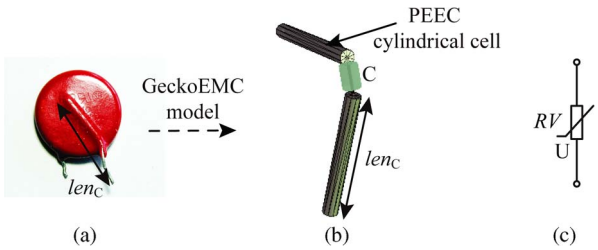

Fig. 8. Metal-oxid varistor (MOV) component: (a) a photograph, (b) PEEC model in GeckoEMC, and (c) circuit symbol.

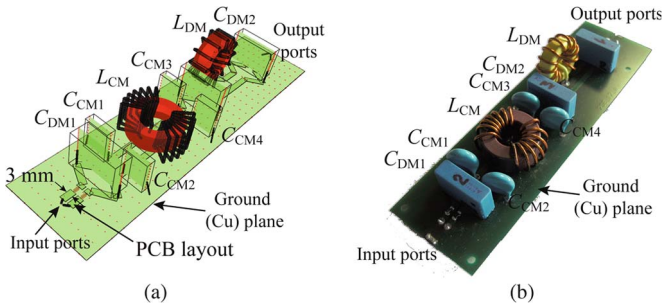

Fig. 9. Two-stage single-phase EMI filter: (a) GeckoEMC model and (b) photograph.

the properties with respect to the measured impedance characteristics in the frequency range of interest. The GeckoEMC models of NTC and RV circuit elements are presented in Figs. 7 and 8, respectively.

B. Modeling of EMI Filter Circuits

To demonstrate the capabilities of the developed 3-D PEEC–BIM EMC modeling approach, the single-phase two-stage EMI input filter, as shown in Fig. 9, was taken as a modeling example.

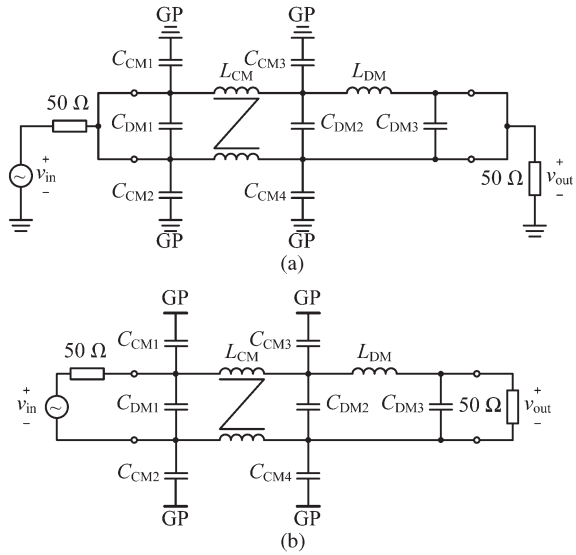

Fig. 10. Single-phase two-stage EMI filter: (a) CM configuration, and (b) DM configuration for measuring; (GP abrevation stands for Ground Plane).

The transfer gain between the input and output ports was simulated and verified by measurements. The transfer function measurements are performed for both CM and DM filter configurations, shown in Fig. 10.

The PCB tracks $(width = 3$ mm$)$ are on the top layer and the copper (ground) plane, GP, is on the bottom layer of the PCB. When the DM attenuation is measured, the GP copper plane behaves as a floating ground plane while for the CM measurements the copper plane GP is connected to the ground of the measurement equipment and provides the return path for the CM currents. The leakage inductance of single-phase CM inductors is used as the DM inductance for filtering DM current noise. The single phase CM inductor is built using a VAC VITROPERM 500F W380 core [43], with a (horizontal) 2×7 winding configuration and a wire diameter of 1.4 mm, $L_{\mathrm{CM,DM}} = 2.4$ μH and $L_{\mathrm{CM,CM}}(\mu = \mu_0) = 5$ mH for $f_{\mathrm{meas}} = 10$ kHz–30 MHz. The DM inductor is built using a Micrometals T94 iron powder -26 cores [44], with 12 turns uniform windings and a wire diameter of 1.4 mm, $L_{\mathrm{DM}}(\mu = \mu_0) = 8.4$ μH for $f_{\mathrm{meas}} = 10$ kHz–30 MHz. The DM capacitors are EPCOS X2 B32923 0.47 μF/305 V with a lead spacing of 22.5 mm [45]. The CM capacitors are MURATA DE1B3KX471KA5B X1/Y1 4.7 nF/250 V with a lead spacing of 10 mm [46]. The permeability curves are extracted from the impedance measurements using the same type of core and applying a lower number of turns N, i.e., $N < 10$, to minimize the capacitive influence of the winding on the measurements of core magnetic properties.

Good agreement between the measurement and the PEEC–BIM simulation (the mismatch is less than 5 dB) is achieved over a wide frequency range, i.e., from low frequencies up to 30 MHz, cf. Fig. 11. The modeled two-stage EMI filter introduces a maximal DM insertion loss of approximately -120 dB, which is at the signal-to-noise limit of the measurement equipment and cannot be accurately measured, cf. Fig. 11(a). The DM transfer gain comprises four resonant frequencies: $f_{\mathrm{R1}} \approx 94$ kHz (due to $C_{\mathrm{DM}} - L_{\mathrm{DM}}$),

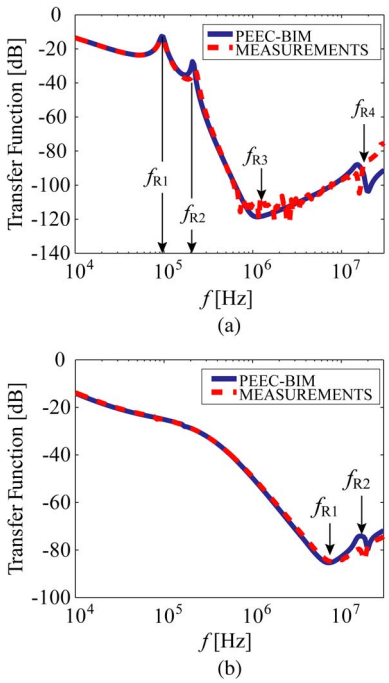

Fig. 11. Comparison between the PEEC simulation and the transfer function measurements of the single-phase two-stage EMI filter shown in Fig. 9: (a) DM attenuation and (b) CM attenuation.

$f_{R2} \approx 0.23$ MHz (due to $C_{DM} - L_{CM,DM}$), $f_{R3} \approx 1.08$ MHz (due to $ESL_{C_{DM}} - L_{DM} - L_{PCB}$) and $f_{R4} \approx 15.2$ MHz (due to $C_{CM} - L_{PCB}$). The CM transfer function is determined by the CM frequency response of the CM inductor, so the first resonant frequency originates from the equivalent parallel capacitance of the CM inductor EPC and the PCB layout, i.e., $EPC_{L_{CM}} - L_{PCB}$, while the second is due to $C_{CM} - L_{PCB}$ resonance, cf. Fig. 11(b).

The measurement 1:1 transformers at the input and output, cf. Figs. 13 and 15, introduce the mismatch between the simulated and the measured transfer gains in the higher frequency range, e.g., above 10 MHz. The measurement setup is described in more detail in the next section.

The placement of the components in practice is significantly influenced by space constraints and EMI filter components often cannot be arranged in an aligned structure as it is shown in the previous example, cf. Fig. 9. Therefore, a practical PCB placement of EMI filter components is modeled and analyzed in the next section.

IV. Modeling of a Practical EMI Input Filter for a PFC Input Stage

The circuit topology, the PCB layout, the GeckoEMC model and the photograph of a single-phase EMI filter for a PFC boost input stage ($V_{in} = 230$ V_{rms}/50 Hz, $P_{out} = 500$ W, $V_{out} = 440$ V) are shown in Fig. 12. The specifications of the filter components are given in Table I. The EMI filter circuit also includes the circuit protection elements: fuses F_1 and F_2, a varistor RV, and a thermistor NTC. The CM capacitors ($C_{CM_1} - C_{CM_4}$) are connected between the power lines ($L_1 - L_4$) and a (ground) PCB track.

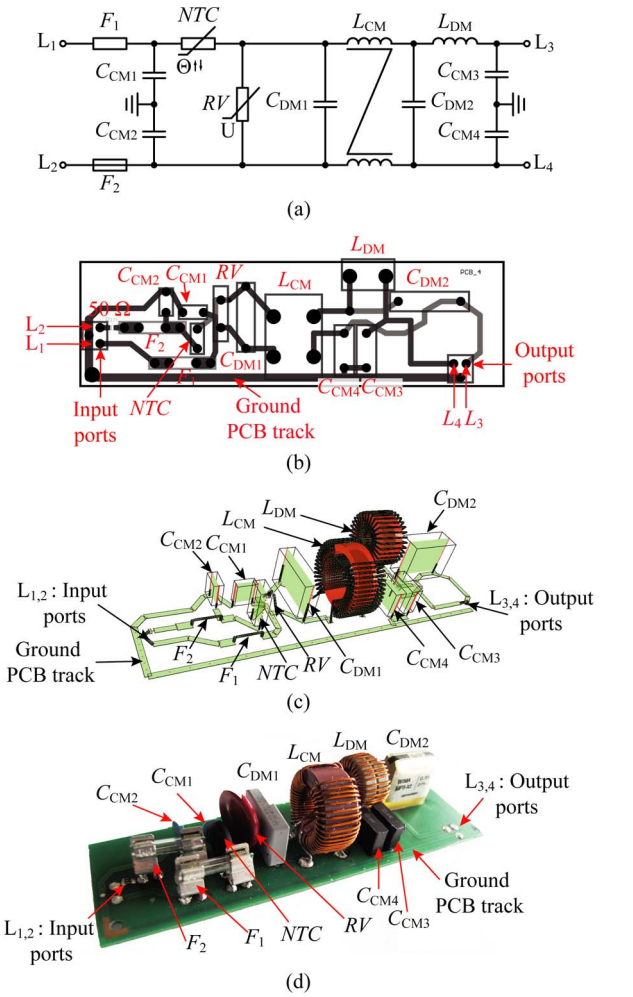

Fig. 12. EMI filter for a single-phase PFC input stage: (a) EMI filter topology, (b) PCB layout, (c) GeckoEMC model, and (d) photograph.

TABLE I
Specifications of EMI Filter Components

Component	Circuit symbol	Specifications/Description
DM (X) capacitors	C_{DM_1}	VISHAY MKP3382, X2 470 nF, 310 VAC [47]
DM (X) capacitors	C_{DM_2}	WIMA MP3-X2, 330 nF, 275 VAC [48]
CM (Y) capacitors	C_{CM_1}, C_{CM_2}	MURATA X1/Y2, 2.2 nF, 250 VAC [46]
CM (Y) capacitors	C_{CM_3}, C_{CM_4}	PANASONIC ECQU3A223MG, X1/Y2, 22 nF, 300 VAC [49]
CM inductor	L_{CM}	VAC VITROPERM 500F nanocrystalline W523 core, single-phase 2 × 20 winding, wire diameter 0.8 mm [43]
DM inductor	L_{DM}	Magnetics two stacked High-Flux 58204A2 cores, uniform 1 × 32 winding, wire diameter 0.8 mm [50]
Fuse	F_1, F_2	Little Fuse, slow blow, 5 × 20, 6.3 A, 250 V [51]
Varistor	RV	TVR20431, metal-oxide, 350 VDC, 275 VAC, 20 mm disk, 700 pF [52]
Thermistor	NTC	Ametherm SL15 4R008 [53]

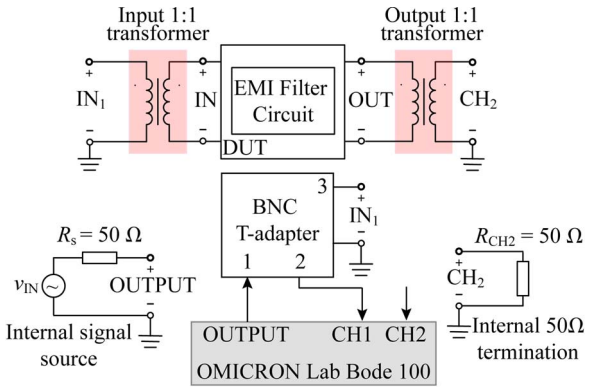

Fig. 13. Schematic of OMICRON Bode100 vector-network analyzer measurement setup.

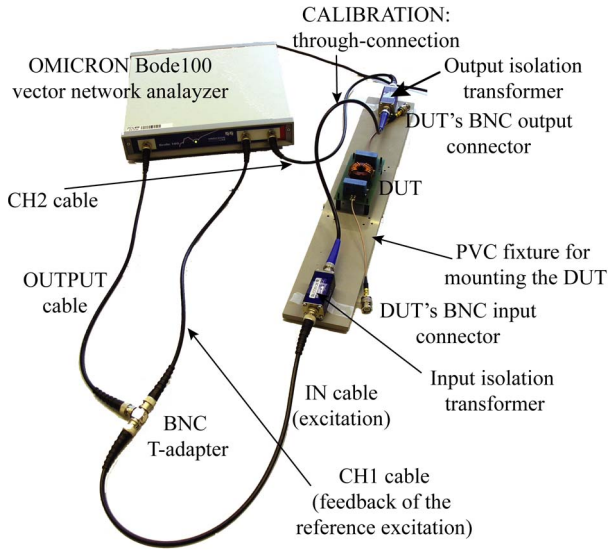

Fig. 14. Photograph of the filter transfer function mesaurement setup.

In the megahertz range, measurement results are very sensitive to any parasitic or EM noise coming from other devices and the measurement equipment itself. Therefore, special attention was directed to building a "good" EMI measurement setup to perform the transfer function measurements with minimal external disturbance. A brief description of the measurement setup is given in the following subsection.

A. Measurement Setup

The measurements setup schematically presented in Fig. 13 consists of an OMICRON Bode 100 vector-network analyzer with an operating frequency range from $f = 10$ Hz to 40 MHz [54]. A photograph of the measurement setup is shown in Fig. 14.

The EMI Filter Circuit block represents the device under test (DUT) including the passive filter components placed onto the PCB. BNC connectors and coaxial cables with a characteristic impedance of 50 Ω are used for the connection between the DUT and the measurement equipment. To match the 50 Ω output impedance of the measurement equipment, 50 Ω resistors are either added onto the PCB layout as SMD components or

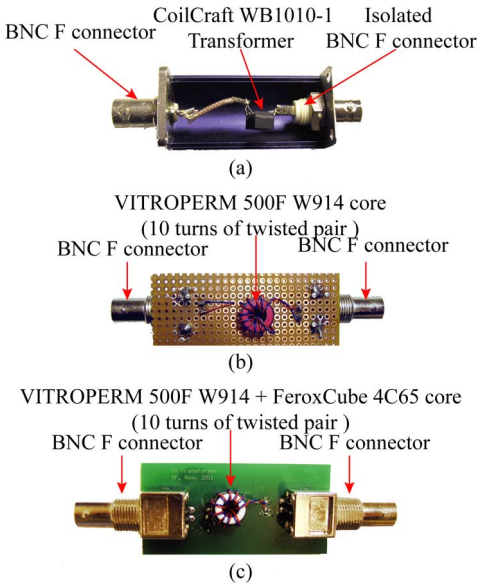

Fig. 15. Input/output 1:1 transformers used in the measurement setup: (a) Transformer 1, (b) Transformer 2, and (c) Transformer 3.

directly soldered to the input/output DUT terminals in series to the signal path. The 50 Ω input resistors are also required in the case of low HF input impedance in parallel to the signal power source to prevent a short-circuit across the signal power source.

The 1:1 input and/or output transformers have to be employed for galvanic isolation between the input and output sides to prevent short-circuiting the series impedance in the ground path across the measurement equipment and also to reduce the shield currents in the coaxial cables. The 1:1 transformers used in the measurements setup are shown in Fig. 15.

These transformers are not needed for the common-mode measurements with the ground plane directly connected to the DUT. The 1:1 transformers should have a low impact on the measured frequency characteristics of the DUT. Namely, the capacitive coupling between the transformer and DUT can introduce disturbance into measurement results. As a transformer is typically designed for a special application, its ideal EM behavior is restricted to a fixed frequency range so that the measurements above and/or below certain frequencies are prone to errors. Specifically, it was observed that both design and position of the transformer can have an impact on the transfer function measurements, which is important to keep in mind when constructing a "good" measurement test setup environment, cf. Fig. 14. The 1:1 transformers are modeled as ideal elements in the 3-D PEEC–BIM simulation so that the transfer gain of the EMI filter under real operating conditions can be evaluated. Three transformers were used in the measurements: **Transformer 1**, a commercial wide-band transformer (CoilCraft WB1010-1 [55], **Transformer 2**, a custom-made transformer (10 turns of twisted pair on a VITROPERM 500F W914 core, wire diameter 0.2 mm) [43] built with approximately two times lower parasitic capacitance between the primary and the secondary windings (10 pF) than the Transformer 1, and **Transformer 3**, a custom-made transformer (10 turns of twisted pair on two stacked cores, VITROPERM 500F W914

TABLE II
INPUT/OUTPUT TRANSFORMERS CONFIGURATION

Measurements	Input Transformer	Output Transformer
no.1	Transformer 2	/
no.2	Transformer 2	Transformer 3
no.3	/	Transformer 3
no.4	Transformer 1	Transformer 3
no.5	Transformer 1	/
no.6	Transformer 1	Transformer 1

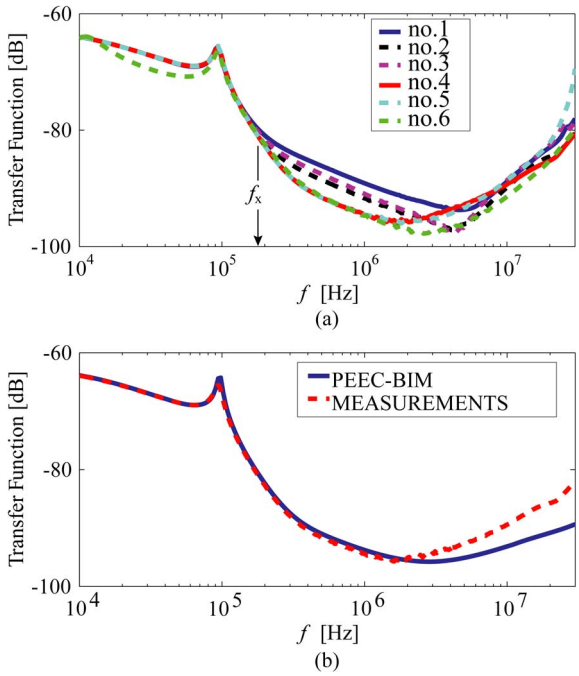

Fig. 16. Comparison of the measurement setups with the 1:1 transformers configurations specified in Table II: (a) measurement results nos.1–4, and (b) PEEC–BIM simulation versus transfer function measurement results no.4

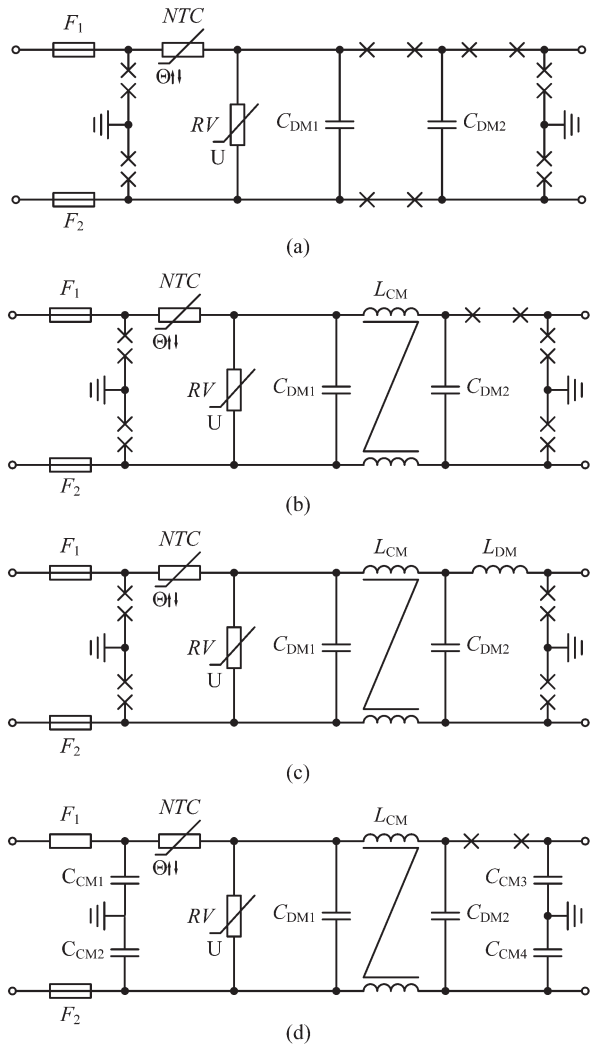

Fig. 17. Step-by-step modeling of EMI filter circuit analyzing the influence of (a) C_{DM}, b) $C_{\mathrm{DM}_1} - L_{\mathrm{CM,DM}} - C_{\mathrm{DM}_2}$ circuit, c) $C_{\mathrm{DM}_1} - L_{\mathrm{CM,DM}} - C_{\mathrm{DM}_2} + C_{\mathrm{CM}}$, and d) $C_{\mathrm{DM}_1} - L_{\mathrm{CM,DM}} - C_{\mathrm{DM}_2} + L_{\mathrm{DM}}$.

core and FerroxCube 4C65 [56], wire diameter 0.2 mm). The influence of the transformers on the measurement results of the EMI filter transfer function is shown and discussed in the next subsection. The calibration of the measurement devices is performed for the through-connection between IN and OUT ports to compensate the cable and connection setup effects.

B. EMI Filter Modeling Results

The disturbance introduced by the measurements setup itself is addressed by performing the transfer function measurements employing different transformer configurations as specified in Table II. The influence of the 1:1 transformers on the measured transfer function of the EMI filter circuit in Fig. 12(a) is presented in Fig. 16. According to the measurement results shown in Fig. 16, the placement of transformers at the input and/or at the output introduces up to approximately 10 dB difference in the measurements in the frequency range above 200 kHz. This can be explained by the non-ideal behavior of 1:1 transformers in the observed frequency range. The PEEC–BIM simulation of the EMI filter transfer function exhibits the best matching to the measurement setup with the 1:1 transformer configuration no. 4, i.e., the commercial transformer at the input and the custom-made transformer at the output side, cf. Fig. 16(b). However, the coupling effect between the DUT and the transformers is pronounced above 10 MHz due to the HF parasitic effects of the transformers.

The DM EMI filter attenuation is simulated in a step-by-step manner to distinguish the influence of individual components on the EMI filter performance. The equivalent circuits are shown in Fig. 17.

The circuit protection components were kept on the PCB in all examples C-I:IV, in Fig. 17. First, only DM capacitors were soldered onto the PCB. Two resonant frequencies originate from the DM capacitors, the parasitic series inductance of capacitors, ESLs and the PCB layout inductances, L_{PCB}. In the second step, the CM inductor was added forming the $C_{\mathrm{DM}_1} - L_{\mathrm{CM,DM}} - C_{\mathrm{DM}_2}$ EMI filter circuit. The comparison of two transfer functions, cf. Fig. 18(a) shows the improvement of the attenuation with the $C - L - C$ filtering. The following two measurements were performed to check the influence of

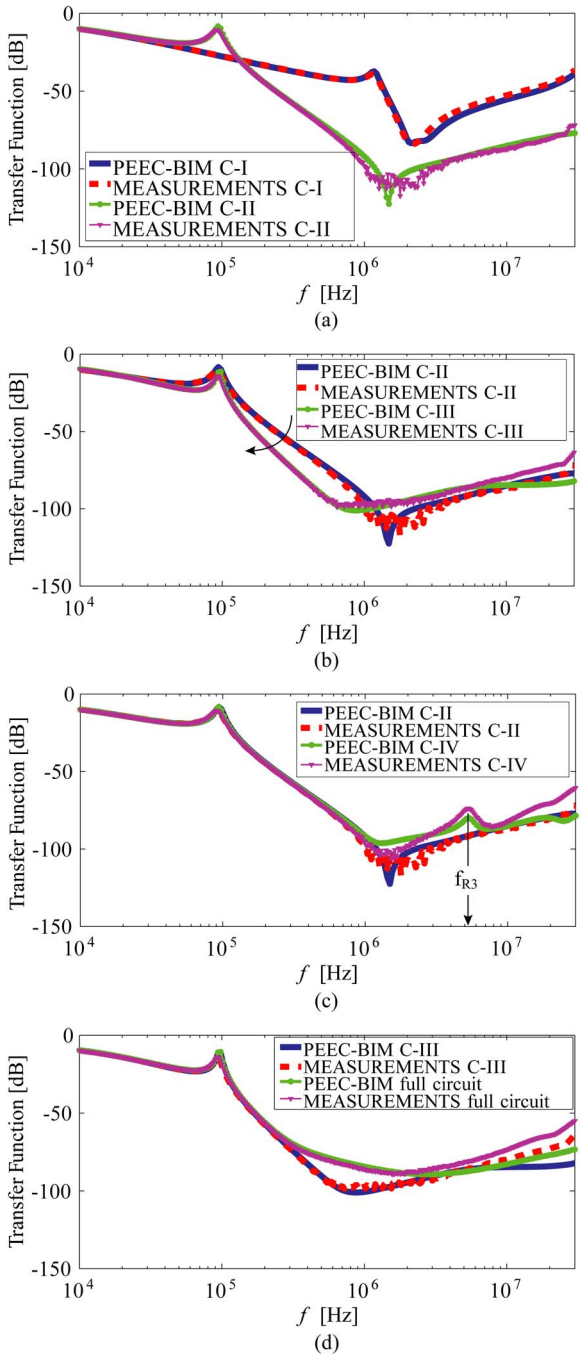

Fig. 18. Comparison of the PEEC–BIM simulation and the measurements of EMI filter circuits presented in Fig. 17 (with (W) and without (W/O) $C_{\rm CM}$): (a) influence of $L_{\rm CM}$, C-I versus C-II, (b) influence of $L_{\rm DM}$, C-II versus C-III, (c) influence of $C_{\rm CM}$, C-II versus C-IV, and (d) influence of $C_{\rm CM}$, C-III versus the circuit with all components.

the DM inductor, cf. Fig. 18(b), and the CM capacitors, cf. Fig. 18(c). As it is shown in Fig. 18, good agreement (less than 10 dB mismatch) between the PEEC–BIM simulation and the measurement results is achieved from dc up to high frequencies, i.e., 30 MHz. Finally, in the last step, the complete DM EMI filter circuit, cf. Fig. 12(a), is modeled and compared to the circuit C-III to check the influence of the CM capacitors $C_{\rm CM_{1-4}}$.

The CM measurements are performed with and without an aluminum (Al) plate $(width = 2\ \text{mm})$ at the distance of 10 mm

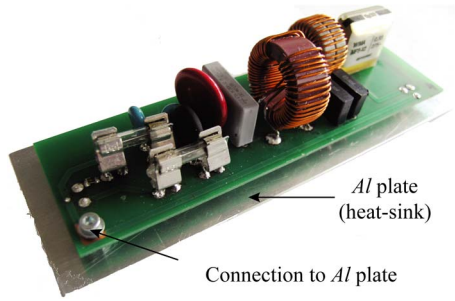

Fig. 19. Photograph of EMI filter circuit connected to an aluminum Al plate.

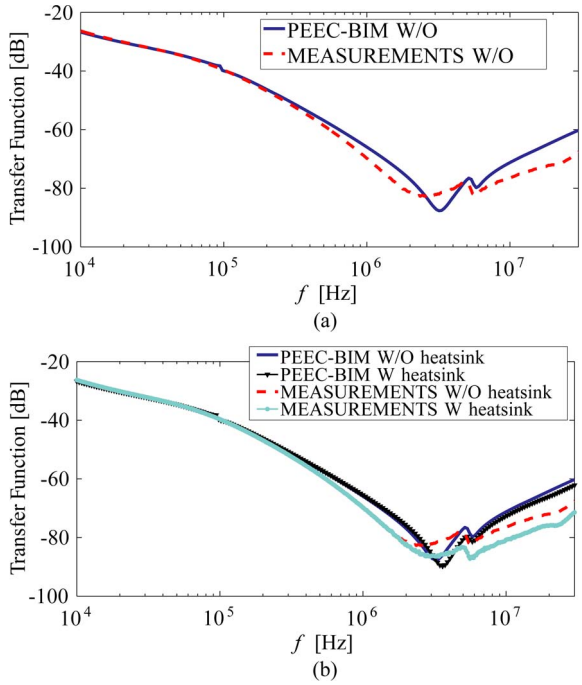

Fig. 20. Comparison between the PEEC–BIM simulation and the transfer function measurements: (a) without (W/O) and (b) with (W) the Al (heat-sink) plate.

from the PCB. The Al plate is connected to the (ground) PCB track as shown in Fig. 19. The presence of the Al plate illustrates the connection to a heat-sink in real EMI filter circuits. In the CM measurements, the ground PCB track is connected to the ground of the measurement equipment, cf. Fig. 10(a). The comparison between the PEEC–BIM simulation and the CM measurement results is shown in Fig. 20. From the measurements, it was observed that CM transfer function is quite sensitive to the input/output connectors and the connection to the ground PCB track in the HF range. The mismatch between the simulation and the measurements in the HF range, i.e., from 10 MHz up to 30 MHz (less than 10 dB), cf. Fig. 20, is the modeling error due to imprecise geometry input parameters, as it is hard to fully describe actual geometry. The increase of EMI CM filter attenuation in the presence of the Al plate, cf. Fig. 20, originates from the electromagnetic field produced by the induced eddy currents in the conductive Al plate.

The influence of the protection circuit elements on EMI filter performance is evaluated by measuring the transfer functions

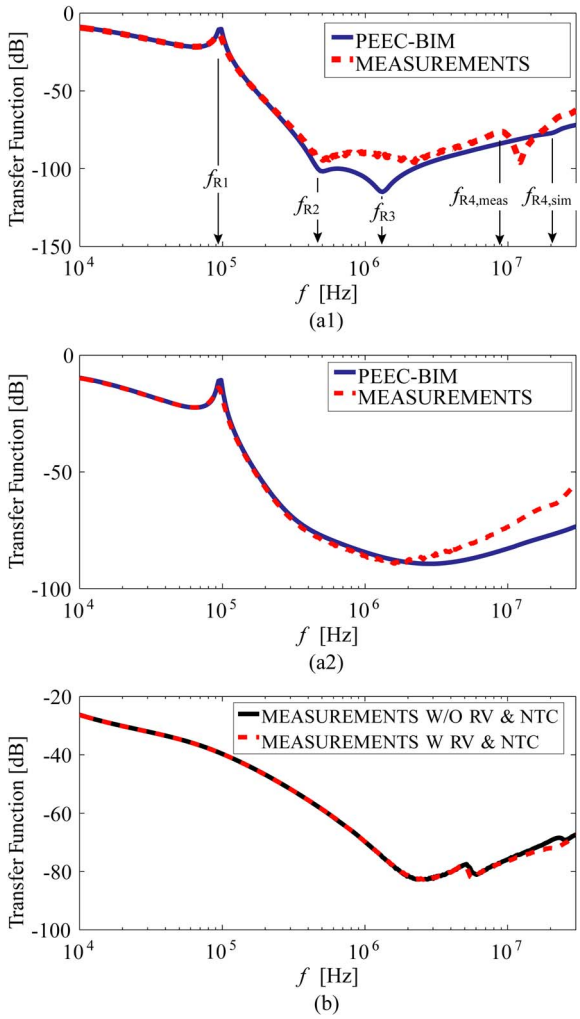

Fig. 21. Comparison between the PEEC–BIM simulation and the transfer function measurements: (a1) DM transfer function without (W/O) RV and NTC, (a2) DM transfer function with (W) RV and NTC, and (b) CM measurements with and without RV and NTC.

of the EMI filters with and without the varistor RV and the thermistor NTC, i.e., replacing RV by an open circuit, and NTC by a PCB track. The EMI filter without RV and NTC comprising only the fuses, F_1 and F_2, introduces a different DM insertion loss above 0.3 MHz than the EMI filter with all protection circuit components, cf. Fig. 21(a1). As mentioned previously, the mismatch between the PEEC simulation and the measurements is due to the sensitivity of the measurement setup, i.e., the transformer parasitics above 10 MHz, and the modeling error of the real geometry. However, it can be stated that the PEEC–BIM simulation results match the measured transfer functions to a high extent and hence, provide useful prediction of the electromagnetic behavior of EMI filter circuits. Similarly, it was observed that the influence of the protection circuit elements on the CM transfer function is not significant in this particular case, cf. Fig. 21(b).

C. EMI Filter Simulation Performance

The mesh of the magnetic surface into N_{M} panels determines the computational complexity and accuracy of the implemented PEEC–BIM method. The simulations were performed on standard PCs with 48 GB RAM and a CPU clock frequency of 2.67 GHz. The calculation time can be separated into the pre-calculation of PEEC–BIM matrix elements and the post-calculation, e.g., the calculation of the transfer function at N_{F} points in the frequency domain. Thus, the PEEC-based modeling of the two-stage single-phase EMI filter presented in Fig. 9 results in a 2012 $\times$ 2012 square system matrix, and requires a simulation time of approximately 11 min: 4 min for pre-calculation and 7 min for post-calculation at $N_{\mathrm{F}} = 201$ frequency points in the range from $f = 10$ kHz to 30 MHz. The good matching between the measurements and the PEEC–BIM simulation results demonstrate that the PEEC discretization enables accurate 3-D modeling of power electronic systems with reasonable computational effort.

V. Conclusion

Power converter systems have to be designed so that low EMI noise emission and necessary EMI noise susceptibility are ensured to meet the EMC standards requirements. Accordingly, the EMC analysis represents an important step of the overall design of power converter systems and has to be performed in early design stages. The EMC analysis is illustrated on the example of a PFC boost converter showing the modeling of EMI noise sources, the modeling of EMI noise propagation paths, and the design of EMI input filter, which is necessary to provide the required EMI noise attenuation. As it has been shown that parasitic effects can degrade EMI filter performances in the HF range, the 3-D EMC modeling represents a highly useful tool for the prediction of EMI filter behavior prior to building hardware prototypes.

The developed 3-D electromagnetic modeling approach is based on the PEEC–BIM numerical technique which enables modeling of magnetic components by means of the linear PEEC-based methodology. In the first step, the PEEC–BIM models of EMI filter components were shown and hereafter, the 3-D modeling of complete EMI filter circuits was presented on two examples: a single-phase two-stage EMI input filter and a practical EMI filter for single-phase PFC input stage. Good matching between the simulated and the measured transfer functions was achieved over a wide frequency range. The measurements were performed using an OMICRON Bode100 vector-network analyzer operating in the frequency range from 10 Hz up to 40 MHz, and with input and/or output 1:1 isolation transformers. It is shown that the comparison between the PEEC–BIM simulation and the measurements with different transformer configurations allows assessing the electromagnetic disturbance introduced by the measurement setup itself.

The EMC simulation enables a step-by-step modeling so that the dominant coupling effects in the HF range can be distinguished leading to an optimal PCB layout and PCB arrangement of EMI filter components. The developed simulation tool GeckoEMC represents an EMC environment for fast and accurate virtual design of EMI filters and power converters and hence, enables the 3-D CAD tool to become the state-of-the-art for practical design of EMI input filters.

REFERENCES

[1] J. Xu and J. Wang, "Bifrequency pulse-train control technique for switching dc-dc converters operating in DCM," *IEEE Trans. Ind. Electron.*, vol. 58, no. 8, pp. 3658–3667, Aug. 2011.

[2] *CISPR 11: Industrial, Scientific and Medical Equipment—Radio-Frequency Disturbance Characteristics—Limits and Methods of Measurement (0, 15–30 MHz)*, Int. Electrotech. Commiss., 1995, 1st ed.

[3] *Electromagnetic Compatibility—Part 3: Limits—Sect. 2: Limits for Harmonic Current Emission IEC 61000-3-2*, Int. Electrotech. Commiss., 1995, 1st ed.

[4] J. P. R. Balestero, F. L. Tofoli, R. C. Fernandes, G. V. Torrico-Bascope, and F. J. M. de Seixas, "Power factor correction boost converter based on the three-state switching cell," *IEEE Trans. Ind. Electron.*, vol. 59, no. 3, pp. 1565–1577, Mar. 2012.

[5] F. Lin and D. Chen, "Reduction of power supply EMI emission by switching frequency modulation," *IEEE Trans. Power Electron.*, vol. 9, no. 1, pp. 132–137, Jan. 1994.

[6] H. Chung, S. Y. R. Hui, and K. K. Tse, "Reduction of power converter EMI emission using soft-switching technique," *IEEE Trans. Electromagn. Compat.*, vol. 40, no. 3, pp. 282–287, Aug. 1998.

[7] G. Spiazzi, S. Buso, M. Citron, M. Corradin, and R. Pierobon, "Performance evaluation of a schottky SiC power diode in a boost PFC application," *IEEE Trans. Power Electron.*, vol. 18, no. 6, pp. 1249–1253, Nov. 2003.

[8] J.-M. Kwon, W.-Y. Choi, and B.-H. Kwon, "Cost-effective boost converter with reverse-recovery reduction and power factor correction," *IEEE Trans. Ind. Electron.*, vol. 55, no. 1, pp. 471–473, Jan. 2008.

[9] K. Mainali and R. Oruganti, "Conducted EMI mitigation techniques for switch-mode power converters: A survey," *IEEE Trans. Power Electron.*, vol. 25, no. 9, pp. 2344–2356, Sep. 2010.

[10] G. Spiazzi and J. A. Pomilio, "Interaction between EMI filter and power factor preregulators with average current control analysis and design considerations," *IEEE Trans. Ind. Electron.*, vol. 46, no. 3, pp. 577–584, Jun. 1999.

[11] A. Baisden, D. Boroyevich, and J. van Wyk, "High frequency modeling of a converter with an RF-EMI filter," in *Conf. Rec. 41st IEEE IAS Annu. Meeting*, 2003, vol. 5, pp. 2290–2295.

[12] S.-P. Weber, E. Hoene, S. Guttowski, J. John, and H. Reichl, "Predicting parasitics and inductive coupling in EMI-filters," in *Proc. 21st Annu. IEEE APEC*, 2006, vol. 1, pp. 1157–1160.

[13] J. Espina, J. Balcells, A. Arias, and C. Ortega, "Common mode EMI model for a direct matrix converter," *IEEE Trans. Ind. Electron.*, vol. 58, no. 11, pp. 5049–5056, Nov. 2011.

[14] K. Ejjabraoui, C. Larouci, P. Lefranc, and C. Marchand, "Presizing methodology of dc-dc converters using optimization under multiphysic constraints: Application to a buck converter," *IEEE Trans. Ind. Electron.*, vol. 59, no. 7, pp. 2781–2790, Jul. 2012.

[15] S. Wang, J. D. Van Wyk, and F. Lee, "Effects of interactions between filter parasitics and power interconnects on EMI filter performance," *IEEE Trans. Ind. Electron.*, vol. 54, no. 6, pp. 3344–3352, Dec. 2007.

[16] S. Wang, Y. Y. Maillet, F. Wang, R. Lai, F. Luo, and D. Boroyevich, "Parasitic effects of grounding paths on common-mode EMI filter's performance in power electronics systems," *IEEE Trans. Ind. Electron.*, vol. 57, no. 9, pp. 3050–3058, Sep. 2010.

[17] S. Wang and F. Lee, "Analysis and applications of parasitic capacitance cancellation techniques for EMI suppression," *IEEE Trans. Ind. Electron.*, vol. 57, no. 9, pp. 3109–3117, Sep. 2010.

[18] S. Wang, F. Lee, and W. G. Odendaal, "Improving the performance of boost PFC EMI filters," in *Proc. 18th IEEE APEC*, 2003, vol. 1, pp. 368–374.

[19] L. Rossetto, S. Buso, and G. Spiazzi, "Conducted EMI issues in a 600-W single-phase boost PFC design," *IEEE Trans. Ind. Appl.*, vol. 36, no. 2, pp. 578–585, Mar./Apr. 2000.

[20] H. Chen and Z. Qian, "Modeling and characterization of parasitic inductive coupling effects on differential-mode EMI performance of a boost converter," *IEEE Trans. Electromagn. Compat.*, vol. 53, no. 4, pp. 1072–1080, Nov. 2011.

[21] L. Yang, B. Lu, W. Dong, Z. Lu, M. Xu, and F. Lee, "Modeling and characterization of a 1 kW CCM PFC converter for conducted EMI prediction," in *Proc. 19th IEEE APEC*, 2004, vol. 2, pp. 763–769.

[22] E. Hoene, A. Lissner, S. Weber, S. Guttowski, W. John, and H. Reichl, "Simulating electromagnetic interactions in high power density inverters," in *Proc. 36th IEEE PESC*, 2005, pp. 1665–1670.

[23] T. De Oliveira, J. Schanen, J. Guichon, and L. Gerbaud, "Automatic layout optimization of an EMC filter," in *Proc. 2nd IEEE ECCE*, 2010, pp. 2679–2685.

[24] Y. Li, L. Luo, C. Rehtanz, C. Wang, and S. Ruberg, "Simulation of the electromagnetic response characteristic of an inductively filtered HVDC converter transformer using field-circuit coupling," *IEEE Trans. Ind. Electron.*, vol. 59, no. 11, pp. 4020–4031, Nov. 2012.

[25] E. Clavel, J. Roudet, T. Chevalier, and D. Postariu, "Modeling of connections taking into account return plane: Application to EMI modeling for railway," *IEEE Trans. Ind. Electron.*, vol. 56, no. 3, pp. 678–684, Mar. 2009.

[26] T.-S. Tran, G. Meunier, P. Labie, and J. Aime, "Comparison of FEM-PEEC coupled method and finite-element method," *IEEE Trans. Magn.*, vol. 46, no. 4, pp. 996–999, Apr. 2010.

[27] I. F. Kovacevic, A. Muesing, and J. W. Kolar, "An extension of PEEC method for magnetic materials modeling in frequency domain," *IEEE Trans. Magn.*, vol. 47, no. 5, pp. 910–913, May 2011.

[28] I. F. Kovacevic, T. Friedli, A. Muesing, and J. W. Kolar, "A full PEEC modeling of EMI filter inductors in frequency domain," presented at the COMPUMAG 2011, Sydney, Australia, 2011, PB11.2 (ID 193).

[29] Gecko-Research, 2012. [Online]. Available: http://www.gecko-research.com/geckoemc.html

[30] I. Kovacevic, A. Muesing, and J. W. Kolar, "PEEC modeling of toroidal magnetic inductor in frequency domain," in *Proc. ECCE ASIA—IPEC*, 2010, pp. 3158–3165.

[31] I. F. Kovacevic, T. Friedli, A. Musing, and J. W. Kolar, "PEEC-based virtual design of EMI input filters," in *Proc. 3rd IEEE ECCE*, 2011, pp. 1935–1941.

[32] I. F. Kovacevic, T. Friedli, A. Muesing, and J. W. Kolar, "Electromagnetic modeling of EMI input filters," in *Proc. 7th Int. CIPS*, 2012, pp. 38–46.

[33] M. J. Nave, *Power Line Filter Design for Switched-Mode Power Supplies*. New York, NY, USA: Van Nostrand, 1991.

[34] W. Zhang, M. Zhang, F. Lee, J. Roudet, and E. Clavel, "Conducted EMI analysis of a boost PFC circuit," in *Proc. 12th IEEE APEC*, 1997, vol. 1, pp. 223–229.

[35] K. Mainali and R. Oruganti, "Simple analytical models to predict conducted EMI noise in a power electronic converter," in *Proc. 33rd IEEE IECON*, 2007, pp. 1930–1936.

[36] T. Nussbaumer, K. Raggl, and J. W. Kolar, "Design guidelines for interleaved single-phase boost PFC circuits," *IEEE Trans. Ind. Electron.*, vol. 56, no. 7, pp. 2559–2573, Jul. 2009.

[37] S. Wang, F. Lee, and W. G. Odendaal, "Characterization, evaluation, design of noise separator for conducted EMI noise diagnosis," *IEEE Trans. Power Electron.*, vol. 20, no. 4, pp. 974–982, Jul. 2005.

[38] P. Kong, Y. Jiang, and F. Lee, "Common mode EMI noise characteristics of low-power ac-dc converters," *IEEE Trans. Power Electron.*, vol. 27, no. 2, pp. 731–738, Feb. 2012.

[39] W. Chen, X. Yang, and Z. Wang, "A novel hybrid common-mode EMI filter with active impedance multiplication," *IEEE Trans. Ind. Electron.*, vol. 58, no. 5, pp. 1826–1834, May 2011.

[40] J. W. Kolar, F. Krismer, Y. Lobsiger, J. Muelethaler, and J. Miniboeck, "Extreme efficiency power electronics," in *Proc. 7th Int. Conf. CIPS*, 2012, vol. 1, pp. 1–22.

[41] C. Zhang, "A PFC with high power factor at low load or high mains voltage," in *Proc. 19th IEEE APEC*, 2011, pp. 56–59.

[42] S. Wang, F. Lee, and J. D. Van Wyk, "A study of integration of parasitic cancellation techniques for EMI filter design with discrete components," *IEEE Trans. Power Electron.*, vol. 23, no. 6, pp. 3094–3102, Nov. 2008.

[43] *Nanocrystalline VITROPERM—EMC Products*, Vacuumscmelze GmbH & Co., Hanau, Germany, 2012.

[44] Micrometals 2012. [Online]. Available: http://www.micrometals.com

[45] EPCOS, 2012. [Online]. Available: http://www.epcos.com/

[46] Murata 2012. [Online]. Available: http://murata.com

[47] Vishay 2012. [Online]. Available: http://www.vishay.com/capacitors/

[48] Wima 2012. [Online]. Available: http://www.wima.com/

[49] Panasonic, 2012. [Online]. Available: http://industrial.panasonic.com/

[50] Magnetics 2012. [Online]. Available: http://www.mag-inc.com/

[51] LittleFuse, 2012. [Online]. Available: http://www.littelfuse.com/

[52] Thinking Electronic Industrial Co. LTD., 2012. [Online]. Available: http://www.thinking.com.tw/

[53] AMETHERM, 2012. [Online]. Available: http://www.ametherm.com/

[54] OMICRON Lab—Bode100, 2012. [Online]. Available: http://www.omicron-lab.com/bode-100.html

[55] CoilCraft, 2012. [Online]. Available: http://www.coilcraft.com

[56] FerroxCube, 4C65 material specification 2012. [Online]. Available: http://www.ferroxcube.com, 4C65 material specification

Ivana F. Kovačević (S'10) received the Bachelor's degree (with honors) from the Department of Electronics, Faculty of Electrical Engineering, University of Belgrade, Serbia, in 2006, and the M.Sc. degree in electrical engineering and information technology and the Ph.D. degree from the Swiss Federal Institute of Technology (ETH) Zurich, Zurich, Switzerland, in 2008 and 2012, respectively, focusing on lifetime modeling of power modules and 3-D electromagnetic modeling of EMI filters.

In June 2007, she joined the Power Electronic Systems Laboratory at the ETH as a postgraduate student, where is currently working as a Postdoctoral Assistant. Her research activities are focused on multi-domain modeling and optimization of power electronics systems and components.

Dr. Kovačević received the Rita Trowbridge Prize from the International Compumag Society for a paper presented at the COMPUMAG Conference 2011.

Thomas Friedli (M'09) received the M.Sc. degree (with honors) in electrical engineering and information technology and the Ph.D. degree from the Swiss Federal Institute of Technology (ETH) Zurich, Zurich, Switzerland, in 2005 and 2010, respectively.

From 2006 to 2011, he was with the Power Electronic Systems Laboratory, ETH Zurich, where he performed research on current source and matrix converter topologies using silicon carbide power semiconductors, active three-phase PFC rectifiers, and conducted electro-magnetic interference. Since 2012, he has been with ABB Switzerland, Ltd., Zurich. He is currently involved in research and development of power electronics and medium-voltage drives for traction converter systems. His research interests are in the areas of high-efficiency power electronic systems and their control, three-phase power converters, electromagnetic interference, and applications of wide band-gap power devices.

Dr. Friedli received the 1st Prize Paper Award of the IEEE IAS IPCC in 2008 and the IEEE TRANSACTIONS ON INDUSTRY APPLICATIONS Prize Paper Award in 2009.

Andreas M. Muesing (M'12) received the degree in physics from the Ruprecht-Karls-University, Heidelberg, Germany, in 2005.

From 2006 to 2012, he conducted his Ph.D. research at the Power Electronic Systems Laboratory, ETH Zurich, Switzerland, where he focused on numerical simulations of power electronics systems. He founded the company Gecko-Research GmbH, Zurich, Switzerland, which he has been leading as CEO since 2010.

Johann W. Kolar (F'10) received the M.Sc. and Ph.D. degrees (*summa cum laude/promotio sub auspiciis praesidentis rei publicae*) from the Vienna University of Technology, Vienna, Austria.

Since 1982, he has been working as an independent international consultant in close collaboration with the Vienna University of Technology in the fields of power electronics, industrial electronics and high performance drives. He has proposed numerous novel converter topologies and modulation/control concepts, e.g.,the VIENNA Rectifier, the SWISS Rectifier, and the three-phase ac-ac Sparse Matrix Converter. He has published over 400 scientific papers in international conference proceedings and over 150 papers in international journals and has filed more than 110 patents. He was appointed Professor and Head of the Power Electronic Systems Laboratory at the Swiss Federal Institute of Technology (ETH) Zurich on Feb. 1, 2001. His current research focuses on ac–ac and ac–dc converter topologies with low effects on the mains, e.g., for data centers, more-electric-aircraft and distributed renewable energy systems, and on solid-state transformers for smart microgrid systems. Further main research areas are the realization of ultra-compact and ultra-efficient converter modules employing latest power semiconductor technology (SiC and GaN), micro power electronics and/or power supplies on chip, multi-domain/scale modeling/simulation and multi-objective optimization, physical model-based lifetime prediction, pulsed power, and ultra-high speed and bearingless motors. He initiated and/or is the founder/co-founder of four spin-off companies targeting ultra-high speed drives, multi-domain/level simulation, ultra-compact/efficient converter systems and pulsed power/electronic energy processing.

Dr. Kolar is a member of the Institute of Electrical Engineers of Japan and of International Steering Committees and Technical Program Committees of numerous international conferences in the field. He is the founding Chairman of the IEEE PELS Austria and Switzerland Chapter and Chairman of the Education Chapter of the EPE Association. From 1997 through 2000 he served as an Associate Editor of the IEEE TRANSACTIONS ON INDUSTRIAL ELECTRONICS and since 2001 as an Associate Editor of the IEEE TRANSACTIONS ON POWER ELECTRONICS. Since 2002 he has also been an Associate Editor of the *Journal of Power Electronics* of the Korean Institute of Power Electronics and a member of the Editorial Advisory Board of the *IEEJ Transactions on Electrical and Electronic Engineering*. In 2011, he was appointed an IEEE Distinguished Lecturer by the IEEE Power Electronics Society. He received seven IEEE TRANSACTIONS Prize Paper Awards and seven IEEE Conference Prize Paper Awards. Furthermore, he received the ETH Zurich Golden Owl Award 2011 for Excellence in Teaching and an Erskine Fellowship from the University of Canterbury, New Zealand, in 2003.